JOURNAL OF MATERIALS SCIENCE 28 (1993) 6247–6260

# Review
# The mechanical failure of oxide scales under tensile or compressive load

M. M. NAGL*, W. T. EVANS
*University of Glamorgan, Department of Mechanical and Manufacturing Engineering, Pontypridd, Mid Glamorgan, CF37 1DL, UK*

Simple mechanical models which could be used to calculate the stresses in an oxide scale on a flat metal substrate are presented. The sources for these stresses and the experimental techniques for measuring stresses and oxide failure are also briefly summarized. The options for stress relief in oxide scales are listed. The importance of lateral oxide growth and oxide plasticity is emphasized. Both processes result in stress relief without scale failure. This is followed by a detailed survey of the proposed mechanisms and models for oxide scale failure under tensile or compressive forces. Experimental evidence in support of these mechanisms is examined and the critical factors for predicting oxide failure are given.

## 1. Introduction

Components operating at high temperatures in aggressive environments have to withstand mechanical and chemical degradation arising from the operating conditions. The mechanical conditions require high static and dynamic strength at operating temperature. Chemical stability requires a high resistance against the attack of oxygen, sulphur, carbon, hydrogen, etc.

Oxide scales are formed at the surface of metal components as a result of a reaction between metal and oxygen at elevated temperatures. Unlike other chemical reaction products, oxide scales can be beneficial in high-temperature applications because they can act as hard resistant surface layers which increase the wear resistance of the materials. Oxides are also chemically stable and act as diffusion barriers, which reduce the rate of further attack. However, in most practical applications these protective layers are stressed, either by externally applied loads, by oxide growth stresses or by thermal stresses induced by the mismatch of the thermal expansion coefficients of oxide layer and substrate. Oxide scales are prone to mechanical failure, because they are ceramic materials, and thus do not have the ductility of the underlying metal [1]. The diffusion barrier function is destroyed when oxide failure occurs which allows the oxygen to regain direct access to the metal. This has the most severe consequences when delamination and spallation of large areas of oxide exposes clean metal surfaces leading to a sharp increase in the oxidation rate and breakaway kinetics.

It is almost impossible to achieve both good mechanical stability of the oxide and a low oxidation rate or a low rate of material consumption, because high mechanical stability requires good deformation properties, i.e. high creep rates. However, the creep rate is determined by the slower moving elements in the oxide, whereas the oxidation rate is determined by the faster moving elements. Therefore, the task is to arrive at the best trade-off between good deformation properties and low rate of material consumption in order to achieve a maximum component lifetime.

There is a large body of published information available on oxides and oxidation of metallic materials. Most of this focuses on the oxidation behaviour of different alloys under specific conditions. In this review only publications on the mechanical stability of oxide layers were considered with particular emphasis on proposed failure mechanisms and models for prediction of failure. The stresses which cause failure were reviewed together with simple mechanical models which could be used to calculate these stresses. Stress-induced oxide growth and plasticity which bypass failure were also discussed. Finally, the merits of different techniques for measuring oxide failure were evaluated before the critical factors for the prediction of oxide failure were discussed.

## 2. Stresses in oxides

Surface oxides grown on metal substrates fail at a critical stress. It is possible to determine the stress by considering the mechanical deformation of the composite. However, the oxide layer is commonly polycrystalline with varying grain structure, mechanical properties, inhomogeneous pore and flaw distribution and an indefinite interface between the metal and oxide [2]. Furthermore, thin layers have

* *Address for correspondence:* Rannesdorf 7, 93449 Waldmünchen, Germany.

0022–2461  

a strong local variation in thickness and external loading stresses are superimposed on to the complex internal growth stresses acting in the oxides [2]. It is clear that such a system is complex. Nevertheless, it is necessary to describe the mechanical deformation of an idealized layer on a metal substrate on the basis of simple assumptions in order to understand the failure mechanisms proposed in the literature and to create a starting point for more detailed models.

In the following section, such a treatment of the mechanical stresses is presented for an idealized oxide/substrate system on flat specimens. The consideration for oxide/substrate systems on circular specimens (i.e. tubes and wires) can be found elsewhere [2]. In addition, the sources of stresses in oxides and their measurement techniques are explained.

## 2.1. Sources of stresses in oxides

Growth stresses arise mainly from the volume change during formation of oxide. It is suggested that if the ratio of volume of oxide to that of metal which it replaces, i.e. the Pilling–Bedworth ratio, exceeded unity, the oxide grows under compressive stress, or vice versa. This only applies to oxide formed at the metal/oxide interface [3]. Growth stresses are mainly compressive because most materials exhibit a volume expansion during oxidation [4, 5]. However, there is still some discussion on how growth stresses develop from the volume change and how some of the stress is relieved during growth [6].

The other most common sources of stresses in oxides are thermal stresses due to cooling/heating or thermo-cycling as a result of differences in thermal expansion coefficients of metal and oxide [7]. Thermal stresses are also induced under thermal shock conditions or when a heat flow is removed [7].

Similarly the substrate geometry can cause stresses, in particular at corners [8, 9]. Finally mechanical stresses can arise in the oxide from axial loading or bending [7].

## 2.2. Mechanical models for stresses in oxides

In the following analysis, plasticity and creep effects are disregarded and elastic isotropy is assumed.

Growth stresses, $\sigma_{gr}$, are a result of volume change during growth, when the expansion of the scale, $\varepsilon_{gr}$, is suppressed without plastic deformation of scale and substrate [2]. The condition of geometrical continuity and constraint for the composite system imposes mechanical stresses of opposite sign in both metal and oxide. The forces in metal and oxide must therefore be in equilibrium

$$\begin{aligned} F_n &= \sigma_m A_m \\ &= -\sigma_{ox} A_{ox} \end{aligned} \quad (1)$$

where the subscripts m and ox stand for metal and oxide, respectively, and $\sigma$ and $A$ are the stress and the cross-sectional area, respectively. Under the condition of elastic oxide and substrate deformation it follows that

$$\varepsilon_{gr} = \frac{\sigma_{ox}}{E_{ox}}(1 - \nu_{ox}) - \frac{\sigma_m}{E_m}(1 - \nu_m) \quad (2)$$

where $E$ is the Young's modulus and $\nu$ is the Poisson's ratio which is $\sim 0.3$ for most metals and oxides during elastic deformation [10]. The condition of constant volume results in a Poisson's ratio of 0.5 for plastic deformation [2].

Combining Equations 1 and 2, the stress in the oxide is

$$\sigma_{ox} = \varepsilon_{gr} E_{ox} \Big/ \left[ \frac{E_{ox}}{E_m} \frac{A_{ox}}{A_m} (1 - \nu_m) + (1 - \nu_{ox}) \right] \quad (3)$$

and in the substrate

$$-\sigma_m = \varepsilon_{gr} E_m \Big/ \left[ \frac{E_m}{E_{ox}} \frac{A_m}{A_{ox}} (1 - \nu_{ox}) + (1 - \nu_m) \right] \quad (4)$$

For very thin oxides or $A_{ox}/A_m \to 0$, Equation 3 can be rewritten as

$$\sigma_{ox} = \frac{E_{ox}}{1 - \nu_{ox}} \varepsilon_{gr} \quad (5)$$

Cooling or thermal strains arise in each layer independently according to $\varepsilon_{th\,ox} = \alpha_{ox} \Delta T$ and $\varepsilon_{th\,m} = \alpha_m \Delta T$, where $\alpha$ is the thermal expansion coefficient and $\Delta T$ is the temperature difference. Both are assumed constant throughout substrate and oxide. If different phases could expand and contract independently, such thermal cycling or cooling would induce no stresses in the system [4]. However, geometrical continuity imposes mechanical strains in both layers. Strain compatibility demands that the total strain in both layers is equal at the interface, or that [4]

$$(\alpha_m - \alpha_{ox}) \Delta T = \frac{\sigma_{ox}}{E_{ox}}(1 - \nu_{ox}) - \frac{\sigma_m}{E_m}(1 - \nu_m) \quad (6)$$

The terms on the right side represent the mechanical strains which arise from the different expansion/contraction of oxide and substrate. A comparison of Equations 2 and 6 shows that they differ only in the term on the left side, i.e. Equations 3–5 can also be used to calculate thermal stress when $\varepsilon_{gr}$ is replaced by $(\alpha_m - \alpha_{ox}) \Delta T$.

The previous models were based on semi-infinite layers. However, actual oxide/substrate systems are of a finite length, $l$. The normal tensile and compressive forces within the layers may then be supported by opposing shear stresses at the interface. If stress relief due to fracture, creep, bending, etc., is ignored, the shear force, $F_s$, in a unit-depth cross-section of the oxide is [4]

$$F_s = h_{ox} \sigma_{ox} \quad (7)$$

where $h_{ox}$ is the thickness. It can be balanced with the

shear stress, $\tau$, at the interface which is

$$F_s = \int_0^{\frac{l}{2}} \tau(x)\,dx = \frac{\tau_{max}}{4} l \quad (8)$$

assuming an elastic situation with the shear stress increasing linearly from zero at the middle of the interface to a maximum at the end [4]. The value for the maximum interfacial stress, $\tau_{max}$, follows using Equations 3, 7 and 8

$$\tau_{max} = 4h_{ox} E_{ox} \varepsilon \Big/ \left\{ l \left[ \frac{E_{ox}}{E_m} \frac{A_{ox}}{A_m} (1 - \nu_m) + (1 - \nu_{ox}) \right] \right\} \quad (9)$$

where $\varepsilon$ is either the oxide growth strain, the thermal strain or the applied strain. The interfacial shear stress increases linearly with the oxide thickness for small values of $A_{ox}/A_m$ according to Equation 9. Therefore, the thicker the oxide, the more likely is oxide spallation via interfacial shear failure. It can also be seen that the oxide length, $l$, is a critical parameter which may vary from the dimensions of the alloy specimen itself, to the very small spacing between through-scale cracks or surface line defects (see also Section 3.3) [4].

Tien and Davidson [4] derived the radius of curvature, the bending stresses and the bending moment which arises if a heat flow from the hotter gas/oxide interface to the colder oxide/substrate interface is present. Such a moment is basically the mechanical action which can cause the oxide buckling phenomenon (see also Section 3.4). Because the oxide is constrained by the substrate a normal stress at the interface will be required to counteract the bending moment.

It is also interesting to note that when multi-layered oxides exist, then neither heat flow, phase transformations or non-homogeneities are needed for oxide buckling, because the differences in thermal expansion of the single oxide phases themselves will provide the bending moment within the multi-layer oxide scale [4]. For example, a double layered oxide should develop a radius of curvature, $\rho$, according to [4]

$$\frac{1}{\rho} = 6(\alpha_2 - \alpha_1)\Delta T(1 + m)^2 \Big/ \left\{ n \left[ 3(1 + m)^2 + (1 + mn)\left( m^2 + \frac{1}{mn} \right) \right] \right\} \quad (10)$$

where $m = h_1/h_2$, $n = E_1/E_2$, and the subscripts 1 and 2 refer to the different phases.

As seen in Equation 10 stress calculation for multi-layered oxides requires a knowledge of the material parameters for each single layer. On that basis, mean values can be calculated treating the structure as a composite [11].

### 2.3. Measurement techniques for stresses in oxides

There is currently no method available to measure the stresses in oxides during mechanical deformation [2]. X-ray strain analysis (X-ray diffraction) has been widely used to determine the residual and growth stresses present within the oxide scales. Other methods are based on the extension of a sample during oxidation or the deflection of a thin metallic strip oxidized on only one surface (deflection method) [12].

## 3. Options for stress relief in oxide scales

The oxide/substrate system can accommodate strain by elastic deformation. If the elastic limit is exceeded, stress relaxation can take place by (i) stress-induced growth processes, (ii) plastic deformation of oxide and/or metal, and (iii) mechanical failure of the composite. Failure can start within the oxide, the substrate or at the interface by delamination [11].

### 3.1. Stress-induced growth processes

Whisker formation is the most common stress-induced growth process and is caused by compressive stresses arising from growth or phase transformation [11]. Similarly, stress-induced lateral oxide growth can increase the critical failure strains during tensile loading with sufficient low-deformation rates [7, 13]. This was observed by Schütze [13] on 18Cr and 24Cr steel during deformation with rates $\leqslant 10^{-6}\,s^{-1}$ at 800 °C. The contribution of lateral oxide growth towards failure strains is difficult to assess. However, a first valuable attempt was made by Schütze [14].

Importantly, both whisker formation and lateral oxide growth relax stresses and maintain the integrity of the oxide during deformation.

### 3.2. Plasticity of oxide scales

Plastic deformation of polycrystalline solids by dislocation glide requires five independent slip systems [15]. However, most of the oxides contain less than five independent primary slip systems [15]. Below a transition temperature, the stresses necessary to activate secondary slip systems are higher than those for the initiation of cracks. Therefore, below this transition temperature only elastic deformation of the oxide occurs before fracture, leading to extremely low fracture strains, unless a sufficiently high hydrostatic confining pressure is applied to prevent crack initiation and allow stresses high enough to activate secondary slip systems [15].

Frost and Ashby [16] analysed a wide range of experimental data on the creep of ceramic materials and developed so-called deformation mechanism maps which summarize the information on the deformation behaviour of a material. These define ranges of dominance for the various deformation mechanisms as a function of applied stress and temperature and yield the resulting strain-rate values. In the maps, cracking is excluded by applying a sufficiently high hydrostatic pressure.

Schütze [15] developed deformation mechanism maps for oxides using the following fields:

(i) plasticity, i.e. low-temperature plasticity due to the motion of dislocation only;

(ii) power law creep, i.e. glide plus climb of dislocations. The diffusion mechanisms of lattice diffusion or dislocation core diffusion were assumed to dominate;

(iii) diffusional flow; mechanical stress can induce a diffusive flux of matter through (Nabarro–Herring creep) and around (Coble creep) the oxide grains [15].

The equations that describe these mechanisms were taken from Frost and Ashby [16]. Schütze [15] also incorporated in these maps the critical stress, $\sigma_c$, at which an oxide would fracture depending on the composite void size (see also Section 3.3), if no hydrostatic pressure is applied which would activate five independent slip systems. Therefore, plastic deformation of the oxide is only possible at stresses less than $\sigma_c$. He obtained good agreement between experimental data and those from the respective maps for aluminium, chromium and nickel oxides [15]. He also argued that the low failure strain values, even at strain rates where creep can contribute to deformation, should not be surprising, because creep causes growth of the physical defects by vacancy transport and vacancy condensation [15]. This increases the value of composite void size $c$ and $\dot{\varepsilon}_c$ (the strain rate below which creep can occur) is decreased. If $\dot{\varepsilon}_c$ falls below the applied strain rate, $\dot{\varepsilon}$, sudden cracking occurs [15]. The void size can increase rapidly during creep due to an interaction or interlinkage of several coplanar physical defects lying close together [15]. The maps can be used to determine the critical strain rate, $\dot{\varepsilon}_c$, below which creep can contribute towards the overall oxide deformation prior to failure. The high strains of 2% found in oxide grown on mild steel (13CrMo44) at 873 K when deformed with a rate of $\sim 10^{-8}\ s^{-1}$ could be explained by plasticity [17]. At the same time, Berchthold *et al.* [17] regarded lateral oxide growth as very unlikely in this case, because oxide growth occurred predominantly by iron diffusion.

One of the important differences between a bulk oxide and an oxide scale seems to be the effect of scale crack healing which gives rise to a type of "pseudo-plasticity" of the scale under certain conditions [15]. Pseudo-plasticity can result from the combination of scale cracking and healing. At low strain rates the rate at which the crack surfaces move apart is lower than the oxide growth rate within the scale crack. Thus, the oxidation processes close the crack more or less instantly [15]. Examples of the healing of through-scale cracks can be found elsewhere [13, 18, 19]. Repeated cracking and healing can result in subsurface depletion of protective scale forming alloying elements [18] and a method for evaluating this process has been suggested [14].

Another form of pseudo-plasticity is quasi "grain-boundary sliding" by microcracking, oxide grain movement, and healing [15]. The critical strain rates assessed for pseudo-plasticity lie above or in the upper range of strain rates encountered in long-term creep tests or under service conditions [15]. Therefore, it is not surprising that quite often macroscopically intact scales are observed even though the scale may have cracked several times [15].

Recent approaches suggest that microcracking can account for missing slip systems in brittle layers, e.g. MgO [2]. Microcracking increases the creep rate but reduces the Young's modulus of the layer [2, 20, 21] giving the layer additional plasticity [20]. This increases the critical failure strain but only as long as the crack-tip stress fields of the uniformly distributed microcracks do not influence each other [11].

Finally, Barnes *et al.* [22] have shown that substrate creep can relieve some of the cooling stresses depending on the cooling rate, the creep properties of the substrate and the ratio of the substrate thickness to oxide thickness.

All the mechanisms given in this section add to the overall deformation that the oxide can undergo before macroscopic failure. Deformation mechanism maps and microscopic observation can identify whether these mechanisms were active under the test conditions. However, at present it is impossible to quantify the strain increment they add to the measured failure strains, which would be vital for accurate predictions of failure.

### 3.3. Failure of oxide scales under tensile stress

Evans [23] proposed a failure mechanism for oxides under tensile stress. Accordingly, first through-scale cracks develop at regions of high stress concentration, i.e. the oxide breaks up into a finite number of segments (Fig. 1). Elastic stress relaxation in the vicinity of these cracks can reduce the local stress concentration within the oxide segment. Plastic stress relaxation within the oxide is possible if sliding can occur at the oxide/metal interface [23]. The shear translation may induce fracture damage at the interface which could result in delamination and subsequent spallation [23]. Another mechanism producing plastic stress relaxation is substrate yielding at the base of through-scale cracks [10]; however, this should not lead to interface delamination. The proposed failure mechanism was confirmed in a recent study of the tensile failure of iron and nickel oxide scales at room and at growth temperature using acoustic emission [24–26].

Linear elastic fracture mechanics has been applied to determine the critical failure strains under tensile stress. This is justified at temperatures where creep is not expected ($T < 0.5T_m$). Through-thickness cracks are likely to develop by propagation of pre-existing defects either within or at the surface of the oxide layer [1, 27]. The critical applied tensile strain, $\varepsilon_c$, needed to produce unstable crack growth is

$$\varepsilon_c = \frac{K_{IC}}{EF(\pi c)^{1/2}} \tag{11}$$

where $K_{IC}$ is the critical stress intensity factor, $c$ is the size of the physical defect (length of a surface defect or half-length of an embedded defect) [15], $E$ is the Young's modulus and $F$ is a numerical factor depending on shape, size and position of the void.

A second approach based on the critical energy release rate, $G_{IC}$, was made by Armitt *et al.* [7] and Robertson and Manning [10]. According to that, frac-

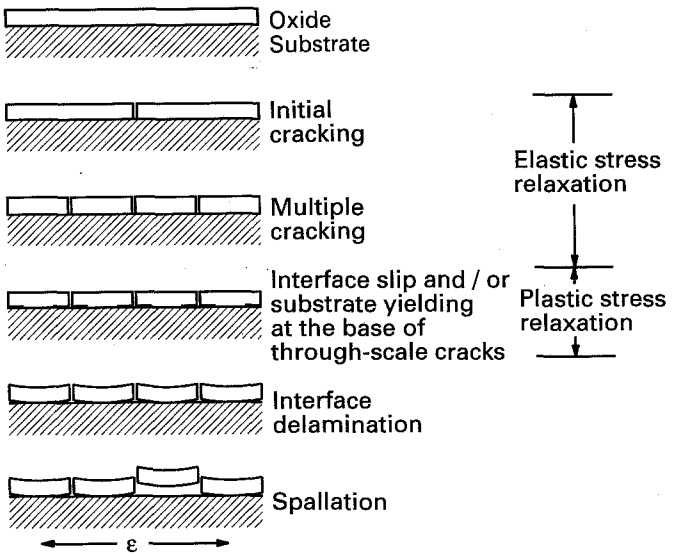


*Figure 1* Schematic diagram of cracking and spallation caused by tensile oxide stress [23].

ture occurs when the energy release rate exceeds a critical value, $G_{IC}$, which is related to the fracture surface energy, $\gamma$, by $G_{IC} = 2\gamma$. This gives the following equation

$$\varepsilon_c = \left(\frac{2\gamma}{F^2 \pi E c}\right)^{1/2} \quad (12)$$

Both approaches are related via

$$G_{IC} = \frac{K_{IC}^2}{E} \quad (13)$$

for the plane stress condition.

In general, two limiting cases govern the relationship between defect size and the thickness of oxide scale [28]:

(i) the defect size is independent of scale thickness, thus the critical failure strains are independent of thickness;

(ii) the defect size is directly proportional to scale thickness.

Robertson and Manning [10] introduced a relationship between the defect size, $c$, and the scale thickness, $h$, which is based on the second condition from above and has the following form

$$c = k h \quad (14)$$

where $k$ is a constant.

Evans and Cannon [29] calculated the lateral extension of a crack initiated at tensile stress concentration sites, e.g. holes, pores, voids and concave undulations at edges. Stable crack propagation occurs when

$$h_c = \frac{2}{\pi}\left(\frac{K_{IC}}{\sigma_{ox}}\right)^2 \approx 0.6\left(\frac{K_{IC}}{\sigma_{ox}}\right)^2 \quad (15)$$

where $K_{IC}$ is the critical stress intensity factor of the oxide, $\sigma_{ox}$ is the stress and $h_c$ is the critical oxide thickness. This is effectively Equation 11 when $c = h/2$ and with an $F$ value of 1.

A final approach to model the scale fracture was made by Grosskreutz and McNeil [30]. They assumed that the substrate deformed by crystallographic slip and that fracture of the oxide may occur at the slip step when the oxide is not strong enough to support the tension necessary to develop the peeling or delamination stresses. It was shown that fracture at the slip step is more likely in thinner films and a thickness of 0.05 μm was given as a dividing line between the fracture at slip steps and tensile fracture by equidistant through-scale cracking for an anodized $Al_2O_3$ layer. In addition, tensile failure strains of 0.1%–0.3% were measured for 0.1–3.0 μm thick films [30]. Schütze [13, 18] investigated the tensile failure behaviour of oxides on alloy 800, 18Cr and 24Cr steel using strain rates between $10^{-6}$ and $10^{-8}$ $s^{-1}$ at 800 °C. The $Cr_2O_3$ layer on alloy 800 did not show lateral oxide growth and the failure strains were $\sim 0.1\%$ when deformed with rates $> 3 \times 10^{-7}$ $s^{-1}$. Lower strains rates allowed some plasticity which increased the failure strain to $\sim 0.5\%$. However, strains of up to 2.5% were found with the scales on the 18Cr and 24Cr steels (containing 0.8 and 1.4 wt % Al and 1.48 and 1 wt % Si, respectively) which showed lateral oxide growth and consisted mainly of $Al_2O_3$.

Following the development of through-scale cracks, further stress relief in response to higher strains can proceed by [7]:

(i) multiple cracking with pure elastic stress relaxation;

(ii) multiple cracking with interfacial slip and/or plastic deformation of the substrate at the base of through-scale cracks;

(iii) delamination at suitable interfaces.

These different cases are discussed below.

### 3.3.1. Multiple cracking with pure elastic stress relaxation

A first approach to determine the increase in crack density has been made by Grosskreutz and McNeil

[30]. They assume that the substrate deforms continuously, and regularly spaced cracks appear in the coating. The spacing, $L$, at any strain, $\varepsilon$, is given by

$$\ln\frac{\varepsilon}{\varepsilon_0} = k\left(\frac{1}{L}\right)\left(\frac{1}{L_0}\right) \quad (16)$$

where $L_0$, $\varepsilon_0$ are any convenient set of data points. The constant $k$ is expected to show a linear or parabolic dependence on the film thickness and must be determined by experiment.

A planar specimen which is undergoing thermal stressing has no shear stresses as long as there is no bending component. Important complications arise at the edges of specimens of finite dimensions (see also Section 2.2), but for the present such edge effects are ignored. There will also be, in reality, a transition zone at the oxide–metal interface where rapid changes in the sign of the stress will occur over short distances [31]. The stress state changes significantly once through-thickness cracks are formed because stresses now develop along the oxide–metal interface [27].

A first attempt to model the shear stress distribution along the oxide–metal interface was made by Tien and Davidson [4] which assumed a linear variation of shear stress with the maximum value at the interface next to the tensile cracks (see also Section 2.2). This gives a limiting crack spacing of

$$L = \frac{4h}{\tau_{max}}\sigma_{ox} \quad (17)$$

For stresses higher than $\tau_{max}$ or $\sigma_{ox}$ fracture will occur at the oxide/substrate interface or within the oxide, respectively.

Evans [27] reviewed this model, together with another which assumed a hyperbolic sine variation of the stress, and compared both predictions for a 10 μm thick $Cr_2O_3$ layer on a 400 μm thick stainless steel sample. The maximum shear stress predicted by the latter was an order of magnitude smaller than that predicted by Tien and Davidson for a crack spacing of 100 μm [27]. In addition, the stress normal to the crack surface drops to zero as soon as a through-thickness tensile crack has developed, thus the tensile stress will vary with position. Again Evans [27] has recently reviewed the two models. Again, he found a significant difference between the two predictions [27].

### 3.3.2. Interfacial slip and/or plastic deformation of the substrate at the base of through-scale cracks

In thin films, interfacial slip provides an option for stress relief over a longer range than the purely elastic relaxation considered above. Armitt *et al.* [7] modelled this situation assuming the shear stress to be constant along the interface. This gave a limiting crack spacing, $L$, of

$$L = \frac{2h\,\sigma_{ox}}{\tau_y} \quad (18)$$

where $\tau_y$ is the shear yield stress of the substrate. Thus, cracking occurs over a range of stresses until the spacing between cracks is of the order of the oxide thickness. Assuming that $\tau_y$ and $\sigma_{ox}$ are of the same order of magnitude, the limiting crack spacing is $2h$, which is half the spacing compared to the case of pure elastic relaxation (Equation 17). In fact, factor 2 in Equation 18 is only an integration constant $\geqslant 2$ which depends on the assumed shear stress distribution in the oxide.

Another valuable attempt to analyse the stress distribution and the interfacial creep processes after cracking has been made by Riedel [32]. He derived a continuum-mechanical equation for thin second-phase layers on deforming metals under plane stress condition, taking into account elastic and creep deformation, as well as stress-independent straining, such as thermal expansion. Linear and non-linear viscous sliding was also allowed at the interface. He used experimental data of Berchthold *et al.* [17] and creep data of Manning [9] to verify the equation. The crack spacing, $L$, was found to decrease with the applied strain rate as $L = k(h/\dot{\varepsilon})^{1/2}$ for small strain rates. In this case $k$ is a constant which has to be determined by experiment. Below a certain minimum strain rate no oxide scale cracking was predicted nor found. It was also concluded that sliding of the scale is controlled by stress-directed diffusion, leading to a linear viscous law rather than by dislocation creep in a thin interface layer, which would lead to non-linear viscous behaviour. However, Barbehön [2] found later that the model cannot be used to predict the crack spacing in nickel oxide when deformed at 800 °C.

Plastic deformation of the substrate at the base of through-scale cracks provides another option for stress relief after initial failure, if one considers the fact that stresses can only be applied to the scale through the metal substrate [10]. Hence, if the substrate itself is strained beyond yielding, no further stress can be applied to the scale. Thus, the strain in the substrate can increase, but the stress in the oxide segments cannot and the metal then accommodates the increase in strain by localized yielding at the base of through-scale cracks [10]. Hence only the crack surfaces move apart. This produces a regime of extended oxide adherence in which the oxide is discontinuous and non-protective, but remains attached to the metal. In practice, the metal yield strain gives only an indication of the boundary of this regime as yielding is not a sudden transition [10]. It is gradual at high strain rates because of work hardening and at high temperatures because substrate creep may reduce work hardening and facilitate interfacial slip [10].

### 3.3.3. Delamination at suitable interfaces

A final option for stress relief following through-scale cracking is crack deflection along a suitable interface, thereby initiating delamination of some or all of the scale [7]. Cracks can develop either at the metal/oxide interface or parallel to it within the oxide layer. However, the deflection of the crack will occur along the surface of lowest energy release rate, $G_{IC}$ [10].

Evans [27] reviewed the possible mechanisms for the crack deflection. Equation 9 suggests that the high

shear stresses which develop at the oxide–metal interface in the vicinity of the crack tips can initiate a shear crack. Tien and Davidson [4] also state that once cracks in the oxide are initiated, $l$ decreases and loss of adherence becomes more likely, i.e. nucleation is the more difficult stage. In contrast, Evans [23, 27] suggested a process of interfacial shear where the interface is expected to develop voids which produce sufficient weakening and which may lead to subsequent delamination. This mechanism is only likely if the shear creep strength of the interface is low. According to Evans, such a situation did arise in the presence of a thin silica interlayer or in cases where the segregation of trace elements has produced a significant weakening of the interface.

Other researchers have investigated the deflection of tensile cracks at interfaces. There is general agreement that the interfacial fracture energy must be less than the cohesive fracture energy [7, 33].

An initial attempt to characterize the failure of oxide in the form of oxide failure maps has been made by Armitt *et al.* [7]. The results of their work have been used in the subsequent work by Robertson and Manning [10]. They found that the thinnest scales fail in a ductile manner because the stress required to propagate a flaw increases as the flaw size decreases. As the scale thickness is an upper limit to the flaw size, reducing $h$ increases $\sigma_c$ until it eventually exceeds the yield stress of the oxide, $\sigma_y$ [10]. This defines the comminution limit of the material using Equations 12 and 14 [10]

$$h = \frac{2\gamma E}{F^2 \pi k \sigma_y^2} \tag{19}$$

In contrast to component testing, where failure occurs once the largest flaw has failed, the presence of a substrate allows an increasing strain to be applied to a scale even after initial cracking [10]. This allows the progressive exploitation of flaws in the scale. Also, as cracks are generated over a wide range of strain levels in the scale, the condition for failure is expected to be described by a spectrum of strain values (Fig. 2) [10].

Schütze [34] established corrosion creep interaction diagrams (CCID), which cover the whole range of strain rates and strain values required for creep, pseudoplasticity, etc., up to fast failure. So far, there have been too few data available to draw a complete CCID for a given material. The purpose of the maps was to find a way of illustrating the interaction of corrosion and mechanical factors in order to divide the whole process of materials degradation into different stages. Some of these stages can be tolerated in practical conditions, others not [34].

It can be seen from the previous analysis that the different proposed models for oxide failure under tension are related to each other even though the starting point or the initial assumptions were quite different. In general, simple linear elastic fracture mechanics was used to predict failure except for very thin scales which might yield or fail at slip steps. The models for subsequent multiple cracking with elastic and plastic stress relaxation show considerable difference in the analysis, and processes such as substrate yielding at the base of through-scale cracks cannot be quantified at all. Several mechanisms were also proposed for the process of interface delamination. However, there are important issues which are yet to be resolved.

Even though the problem of oxide failure in tension has been discussed in many publications, experimental data are very limited and when obtained mainly bulk oxides were used. Some data, however, are available on thermally formed scales using very low strain rates, $\leqslant 10^{-6}\ s^{-1}$, where lateral oxide growth or creep was possible [13, 17]. Even then there was no discussion of the oxide thickness or the void size which are both very important parameters.

## 3.4. Failure of oxide scales under compressive stress

Fig. 3 shows the observed failure mechanisms, together with the designation and the critical condition for initiation. Cases B and E are similar, except that for Case E the oxide delaminates along a line of least cohesive strength within the oxide. In Case C a shear crack develops under 45° as a result of shear failure. This failure mechanism was observed in NiO [2, 35]. In Case D the oxide delaminates as a result of grain-boundary sliding in the substrate adjacent to the interface. This can also lead to tensile failure as suggested by Grosskreutz and McNeil [30] (see also Section

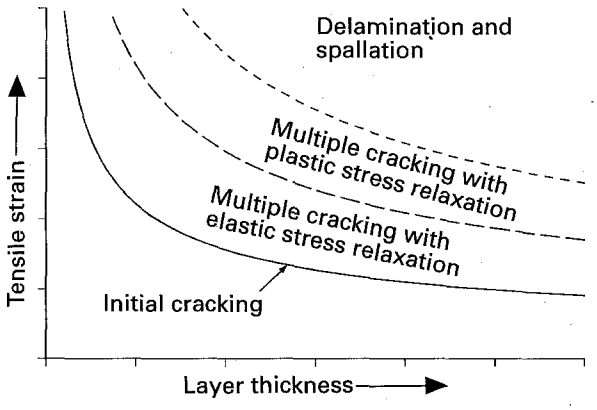


*Figure 2* Schematic failure mode map for oxides tested in tension showing the different stages of the failure process.

| Designation | Critical initiation condition | Schematic diagram of the failure mechanism | Ref. |
|---|---|---|---|
| Case A: Route I (shear failure by wedging) | Critical shear strength | | [37] |
| Case B: Route II (buckling) | Critical buckling stability | | [36] |
| Case C: (shear failure) | Critical shear strength | | [2] |
| Case D: | Substrate yielding | | [30] |
| Case E: | Critical buckling stability | | |

*Figure 3* Schematic diagram for different oxide failure mechanisms which were observed in oxides under compressive stress after [2].

3.3). Case A, termed Route I or wedging, was originally proposed by Evans [23]. It is characteristic of a strong interface and a weak oxide. Oblique shear cracks are initiated within the oxide. The sliding of the oxide along these cracks during further straining drives the oxide away from the substrate and finally it spalls off [23]. Case B, termed Route II or buckling, was originally proposed by Wells *et al.* [36]. It is the result of a weak interface and a relatively strong oxide [23]. An initial delamination originates along areas of loose interfacial strength, i.e. along pores, voids and impurities. This initial delamination or buckle creates a driving force causing the delamination to extend in both directions along the interface. Tensile cracks develop when the buckle reaches a critical curvature and the oxide spalls off [23]. In both routes, the cracks parallel to the interface propagate along the area of least adhesive/cohesive strength, which can be either within the oxide scale or along the substrate/scale interface [10].

A first approach to understand the spallation process was made in 1948 by V. R. Evans. He proposed that oxide–metal debonding would occur when the strain energy within the oxide layer was equal to, or exceeded, the interfacial fracture energy. The idea has been developed by a number of researchers [4, 7, 10, 23, 27, 37, 38].

The stored energy, $W^*$, per unit volume of the layer is

$$W^* = \frac{1}{2}\sigma_1\varepsilon_1 + \frac{1}{2}\sigma_2\varepsilon_2 = \frac{\sigma_{ox}^2}{E_{ox}}(1-\nu) \quad (20)$$

where $\sigma_i$ and $\varepsilon_i$ are the principal stresses and strains, respectively. $E_{ox}$ is the Young's modulus, $\sigma_{ox}$ is the stress in the oxide and $\nu$ is the Poisson's ratio of the oxide. The energy release rate, $G_{IC}$, for cohesive failure is

$$G_{IC}^{cohesive} = 2\gamma_{ox} \quad (21)$$

where $\gamma_{ox}$ is the fracture surface energy value of the oxide and the factor of 2 accounts for the fact that two new surfaces were created. Equation 21 is applicable for Route I and Route II failure if delamination takes place within the oxide [39]. If delamination takes place at the oxide/metal interface, the energy release rate, $G_{IC}$, for adhesive failure becomes [37]

$$G_{IC}^{interface} = (\gamma_{ox} + \gamma_m - \gamma_{interface}) \quad (22)$$

where the subscripts, ox and m stand for oxide and metal, respectively and $\gamma_{interface}$ is the stored energy due to the constraints at the original metal/oxide interface. Because $G_{IC}^{interface}$ contains contributions from both the fresh oxide and the metal surface, it is not necessary to include a factor of 2 [37]. For Route I failure, Evans and Lobb [37, 38] derived the strain $\varepsilon_I^{init}$ to produce a single shear crack of the length $\xi$ as

$$\varepsilon_I^{init} = \left[\frac{G_{IC}^{cohesive}}{k_1\xi E_{ox}(1-\nu)}\right]^{1/2} \quad (23)$$

where $k_1(\ll 1)$ is a factor related to the fraction of stored energy within the layer that is used for the fracture process. Spallation occurs only when the shear crack is deflected at the interface, i.e. the oxide is driven away from the substrate by the wedging effect of the shear crack surfaces. Thus, a second criterion was required to account for the initiation of spallation, $\varepsilon_I^{spall}$ [37, 38]

$$\varepsilon_I^{spall} = \left[\frac{G_{IC}^{interface}}{k_2 E_{ox} h(1-\nu)}\right] \quad (24)$$

where $h$ is the oxide thickness and $k_2(\sim 1)$ is the stored energy in the volume $\xi^2 h$ used in the fracturing process.

Route II behaviour is also described by two equations. In this case the first equation governs the initiation of buckling and the second the initiation of spallation.

Two aproaches have been made. In the first, the critical compressive stress to initiate buckling was approximated by that to produce buckling of a clamped, circular plate of radius $R$ (which equates in this context to the radius of the initial decohesion). Thus, the critical buckling strain, $\varepsilon_{II}^{init}$, is given as [40, 41]

$$\varepsilon_{II}^{init} = \frac{1.22}{(1-\nu^2)}\left(\frac{h}{R}\right)^2 \quad (25)$$

where $2R$ is the diameter of the initial decohesion. However, in order to initiate spallation without unstable propagation of the buckled zone, it remains necessary for tensile cracks to develop at regions of high curvature within the buckle so that a fragment of the oxide layer can be released [41].

A second approach has been made by Wells *et al.* [36] who defined the spall criterion as that to initiate unstable propagation of the buckle. This is expected to give an upper limit to the spallation strain, $\varepsilon_{II}^{spall}$, of [36, 37, 41]

$$\varepsilon_{II}^{spall} = \left(\frac{1.052h^4}{R^4} + \frac{1.041G_{IC}}{E_{ox}h}\right)^{1/2} \quad (26)$$

where the value of $G_{IC}$ depends on the energy release rate at the plane of delamination. The first expression in Equation 26 governs the initiation, and the second the spallation. A comparison of the second term with Equation 24 shows that they differ only by a numerical factor, indicating that spallation is governed in both cases by the propagation of a tensile crack at the interface [41]. Equations 25 and 26 also indicate that it becomes more difficult to buckle as the oxide thickness increases (Fig. 4). Furthermore, the presence of an initial delamination does not disturb the stress field until the oxide layer has buckled, i.e. a driving force for buckling must exist [41]. Such driving forces can be heat flow and thermal expansion of multi-layered scales [4] (see also Section 2.2). Likewise, compositional changes in a single layer can cause differential stresses.

Evans and Lobb verified their models in tests with 20Cr austenitic steel oxidized at 1123 and 1173 K and controlled cooling (rate 86 K $h^{-1}$). The mass gain during pre-oxidation up to 1500 h and during cooling was recorded using a microbalance. The tests showed cracking and spalling above a critical threshold mass gain or thickness. An initial increase in mass at the

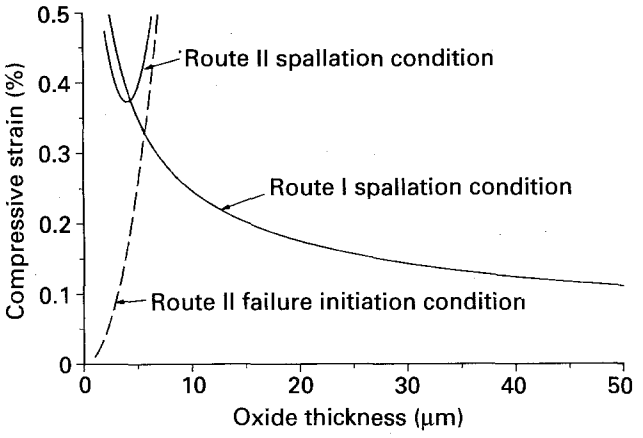


*Figure 4* Comparison of the compressive failure strain as a function of thickness predicted from models, after [38]. $R = 100\ \mu m$, $\nu = 0.3$, $E_{ox} = 210$ GPa, $\gamma_{ox} = 4.5\ J\,m^{-2}$ or $G_{IC} = 9.0\ J\,m^{-2}$.

beginning of cooling was interpreted as a loss of protection of the surface film due to cracking [38]. The release of spalled particles occurred subsequent to this stage and so identified the process of spallation as Route I. This was supported by metallographic observations showing inclined fracture surfaces in the remaining oxide on the 20Cr austenitic steel containing 0.56 wt % Si [42]. The strain, i.e. temperature drop at which spallation of 0.5% of the oxide occurred decreased for all test conditions with increasing oxide thickness according to the predictions of Equation 24 [23]. Evidence for Route II buckling was found in the spalling of oxide grown on an aluminide coating during high-frequency cyclic testing in a burner rig [36] and in 20Cr austenitic steel with low silicon-content [42]. Route I and Route II mechanisms were also found during compressive failure of brittle lacquer and iron oxide scales $< 12\ \mu m$ thick at room temperature, respectively [39]. Thicker iron oxide scales showed only interface delamination, but this was due to the particular oxide geometry [39].

The feasibility of Route I and II failure was also demonstrated by a finite element analysis undertaken on the same steel and test conditions by Evans *et al.* [41]. It was assumed that the oxide behaved elastically and the creep response was determined by the properties of the substrate. In fact, the model which included creep relaxation agreed better with the experimental data and a value of $1\text{–}2\ J\,m^{-2}$ was found for the fracture energy of the oxide–metal interface, which is one to two orders of magnitude higher than that expected for purely elastic deformation [41]. This suggested that the substrate creep properties determine the rate of the interfacial crack growth.

Robertson and Manning [10] used the geometrical approach of linear elastic fracture mechanics with $K = \sigma h^{1/2}$ for a long crack below a strip of thickness $h$ [10, 43]. Together with Equation 13, the critical failure strain, $\varepsilon_c$, becomes

$$\varepsilon_c > \left(\frac{G_{IC}}{hE}\right)^{1/2} \tag{27}$$

which corresponds to the model proposed by Armitt *et al.* [7] and is very similar to the failure criterion under tensile stress. In addition, a comparison with Equation 24 shows that both agree up to a numerical factor, indicating that linear elastic fracture mechanics could be used to model interface delamination in oxides. However, the situation is more complex because the tensile crack at the interface represents a crack showing partly elastic behaviour in the oxide and partly plastic behaviour in the substrate. At present, the situation at the crack tip and its plastic deformation cannot be determined mathematically; only finite element modelling can be used to determine stresses and strains at the crack tip.

Schütze [44] criticized this model (Equation 27) because it does not take account of the size of possible defects at the interface or within the oxide. He used, therefore, a model which was originally proposed by Evans *et al.* [31] to calculate the interfacial strain that arises from the compressive loading of a wavy interface. Assuming that the substrate deforms plastically, i.e. $\nu_m = 0.5$, the maximum strain normal to the interface is [44]

$$\varepsilon_n^{max} = \varepsilon m \Big/ \left(1 + \frac{r}{h}\right) E_{ox} \tag{28}$$

where $\varepsilon$ is the applied compressive strain, $r$ characterizes the amplitude of the wavy interface, $h$ is the mean scale thickness and $m$ is a constant given by $m = 2E_{ox}/(1 + \nu_{ox})$. Assuming the worst case, that the physical defect size $2c$ lies at the position of maximum interfacial strain, a combination of Equations 11 and 28 gives the critical applied compressive strain

$$\varepsilon_c = \frac{K_{IC}}{F(\pi c)^{1/2}} \left(1 + \frac{r}{h}\right) \Big/ m \tag{29}$$

Tien and Davidson [4] proposed a simple buckling model for thin oxides by the way of critical buckling. From beam theory, a single beam which is pinned only at the ends can suddenly buckle at a point of instability when the axial compressive stress exceeds a critical value. However, this model appeared too crude an approximation for the situation of an oxide layer on a metal substrate.

It was found by Evans *et al.* [23, 45] that continued cooling increased strain levels within the oxide layer, which led to further spallation. Such an increase was interpreted by different areas of the specimen surface reaching their critical energy value for spallation [23]. It was believed to be a result of the combined intrinsic variation in both fracture energy, $G_{IC}$, and oxide thickness [45]. After fractional oxide losses of 30%–40% the spallation rate decreased due to stress relaxation in the residual oxide. This approach was quite different from the proposal of Schütze [44]. It implied that $G_{IC}$ could vary within the oxide. However, Schütze proposed that $G_{IC}$ is constant and that the variation in the critical strain energy to cause spallation was solely due to the void size. This is very similar to what was found in tension, but it would require a detailed assessment of the voidage at the interface which is difficult to achieve.

To date there has been little experimental data to support one or the other failure mechanism. Quite

often the results were only obtained in thermo-cycling or cooling experiments rather than under applied load. Regardless of the different lines of thought, all proposed failure mechanisms have an initiation condition and a spallation condition. The spallation condition is, in all cases, the same. It requires crack propagation along the interface or within the oxide parallel to the interface. Reference to Fig. 3 and the preceding analysis shows that initiation can only occur when the stress exceeds the shear strength of the oxide (Cases A and C), the buckling stability of the oxide layer (Cases B and E) or when the substrate yields (Case D).

## 4. Measurement methods for oxide scale failure

To date, four different methods have been used to detect scale cracking. These were optical methods, thermogravimetry, vibration technique and acoustic emission.

Optical methods, using a long focal length microscope and a stage having heating and loading facilities, can be used to detect scale cracking [14, 17]. However, the spatial resolution is only limited ( $\sim$ 0.5 μm). Thermogravimetry is normally used to monitor mass gains during oxidation in order to measure rates of oxidation. It can also reveal through-scale cracking which manifests itself in a sharp increase in mass or oxidation rate and scale spallation which produces a sudden mass loss [38]. However, it is restricted to metal/oxide systems where mass changes caused by scale cracking can be readily detected [3]. The vibration technique monitors the change in the natural frequency of a freely suspended specimen. The natural frequency of the specimen depends on the oxide and substrate dimensions, i.e. stiffness. Therefore, monitoring the natural frequency changes can yield information about the oxide thickness [46]. It can also be used to detect the onset of scale cracking, because crack formation results in a reduction of stiffness of the composite system and hence a discontinuity in the resonant frequency is observed. Continued cracking would result in a continual decrease in the recorded frequency [3]. Should scale repair occur, then a change in frequency is observed with the frequency recorded after repair approaching that observed before cracking. However, this technique is limited to simple rod-shaped specimen geometries and requires care in preparing and setting up the specimens [3]. Acoustic emission (AE) has been known for many years as a remote monitoring technique which can be used to record acoustic waves generated by the sudden release of strain energy during plastic deformation or cracking. Detection of fracture processes at high temperatures can be achieved by placing the transducer away from the source of emission, e.g. outside the furnace. AE can be monitored automatically, is not limited to particular specimen geometries and has similar sensitivities to scale cracking (Fig. 5) [3, 47]. It has recently replaced the vibration technique as a route to measure *in situ* early scale failure [18, 24–26, 47–50], although, an additional advantage of the vibration technique is that the Young's modulus can also be determined *in situ* [3].

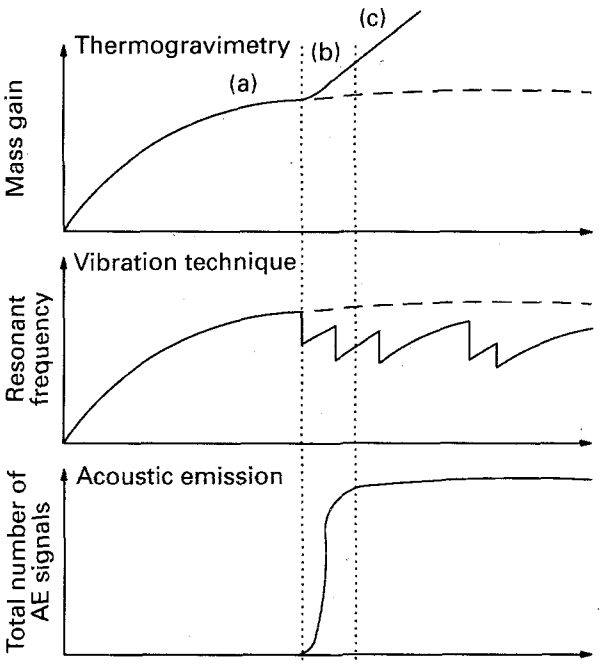


*Figure 5* Schematic diagram showing the response to breakaway oxidation. (a) Normal oxidation, (b) initial cracking, (c) continued cracking and crack repair [3].

## 5. Discussion of critical parameters for prediction of oxide scale failure

The preceding analysis demonstrated the critical parameters governing tensile and compressive oxide failure. These are the Young's modulus, the fracture surface energy of oxide and interface, the composite void size, the overall state of stress, the effects of lateral oxide growth, plasticity and creep of oxide and substrate.

Table I gives a summary of oxide parameters. It also demonstrates the scatter of the values found in the literature. Young's modulus values and surface energy values have recently been provided by Robertson and Manning [10]. A value of 0.04 nm for $\gamma/E$ was given for a range of polycrystalline ceramic materials and $\gamma$ varied between 4 and 40 J m$^{-2}$ [7]. The relationship between $\gamma$ and $E$ was also found by Robertson and Manning [10] for polycrystals, but with a constant value of 0.02 nm.

In all models, spalling will occur along the surface of lowest energy release rate, $G_{IC}$, which can be either within the scale or along the scale/metal interface. This leads to the question of whether or not the interface is intrinsically weak [10]. Robertson and Manning [10] have pointed out that the scale/metal interface is intrinsically strong on an atomic scale and models for estimating the increase of the interface surface energy with increasing interface roughness have been proposed [10, 51]. On the other hand, the scale/metal interface is also a site for segregation of elements which are relatively insoluble in the scale or for oxides which have the highest thermodynamic solubility at low oxygen partial pressures, e.g. $SiO_2$

TABLE I Summary of oxide parameters from various references. $\gamma_{th}$ is the theoretical surface energy which was calculated using Coulombic potentials and allowing for some relaxation of atomic positions at the surface [10]; $\sigma_{cool}$ is the cooling stress

| Material | Temp. (°C) | Young's modulus (GPa) | Growth stresses (MPa) | $\alpha_{oxide}$ ($10^{-6}$ K$^{-1}$) | Surface energy (J m$^{-2}$) | Reference | Notes |
|---|---|---|---|---|---|---|---|
| Oxide on Armco iron | 500 | 192 | | | | | 0.2% C steel |
| | 600 | 178 | | | | | |
| | 700 | 164 | | | | [54] | |
| | 800 | 151 | | | | | |
| | 850 | 144 | | | | | |
| $Fe_2O_3$ | 20 | 220 | | 13 | 6.0 | | $\gamma_{th}$ = 2–2.3 |
| $Fe_3O_4$ | 20 | 210 | | 12 | 4.5 | [10] | $\gamma_{th}$ = 1.5–2.2 |
| FeO | 20 | 130 | | 15 | 3.0 | | $\gamma_{th}$ = 0.94 |
| $Fe_2O_3$ | 20 | 122 | | | | | Scale |
| | | 205–266 | | | | [7] (from | Bulk oxide |
| $Fe_3O_4$ | 20 | 140–260 | | | | various refs) | Scale |
| $Fe_3O_4$ + 20% $Fe_2O_3$ | 20 | 61–84 | | | | | |
| FeO | 570–800 | 190–120 | | | | | Mainly FeO |
| FeO | 20 | 128 | | | | | Bulk oxide |
| FeO | 600–900 | 75 | | | | | Mainly FeO |
| $Fe_3O_4$ + $Fe_2O_3$ | 500 | | ± 100 | | | [55] | |
| NiO | 20 | 220 | − 400 | 1.03 ($\alpha_{ox}/\alpha_m$) | | [5] | |
| NiO | 20 | 190 | | 17.1 | 3.6 | [10] | $\gamma_{th}$ = 1.15–2.77 |
| NiO | 900 | | 335 | | | | 5.4 μm |
| | | | 300 | | | | 12.1 μm |
| | | | 240 | | | [56] | 18.1 μm |
| | | | 185 | | | | 25.2 μm |
| | | | 85 | | | | 32. μm |
| NiO | 900 | | ± 50 | 17.6<br>0.82 ($\alpha_{ox}/\alpha_m$) | | [57] | $\sigma_{cool}$ = 0–500 MPa |

with respect to a $Cr_2O_3$ scale [10]. Similarly, sulphur segregation was assumed to have a negative influence on the interface strength [29]. It is difficult to separate each of these aspects at the present state of experimental knowledge [10, 14].

Evans and Lobb [38] obtained an interfacial energy value of 5.8 J m$^{-2}$ for a $Cr_2O_3$ layer on 20Cr austenitic steel. Evans and Lobb [45] also gave an average value of about 40 J m$^{-2}$ for 50% spallation for the same oxide and a value of 1–2 J m$^{-2}$ which was obtained by a finite element analysis [41]. A value of 11.5 J m$^{-2}$ for $G_{IC}$ was found for a fractional loss of 50% for the outer layer scales ($Fe_2O_3$) on Type 316 steel [7] and it was assumed that it is the same for ferritic and austenitic steels. Robertson and Manning [10] also obtained good results assuming an idealized interface with a surface energy value equal to that of the oxide, i.e. $G_{IC}^{adhesive} = G_{IC}^{cohesive}$ and methods for measuring $G_{IC}^{interface}$ have been suggested [14].

So far, little attention has been directed towards the effects of voids within the oxide or at the oxide/metal interface on the failure process, although it is an important factor in all the quoted models for through-scale cracking and spalling. Recently, a method for evaluating the composite void size in an oxide containing multiple randomly scattered voids and pores was proposed by Hancock and Nicholls [1]. The analysis follows guidelines used for the assessment of defects in welds and requires that each defect is idealized and compared with its neighbours to assess whether the interaction conditions apply (Fig. 6). Interacting defects are considered as a single defect and the assessment procedure continues, until a single

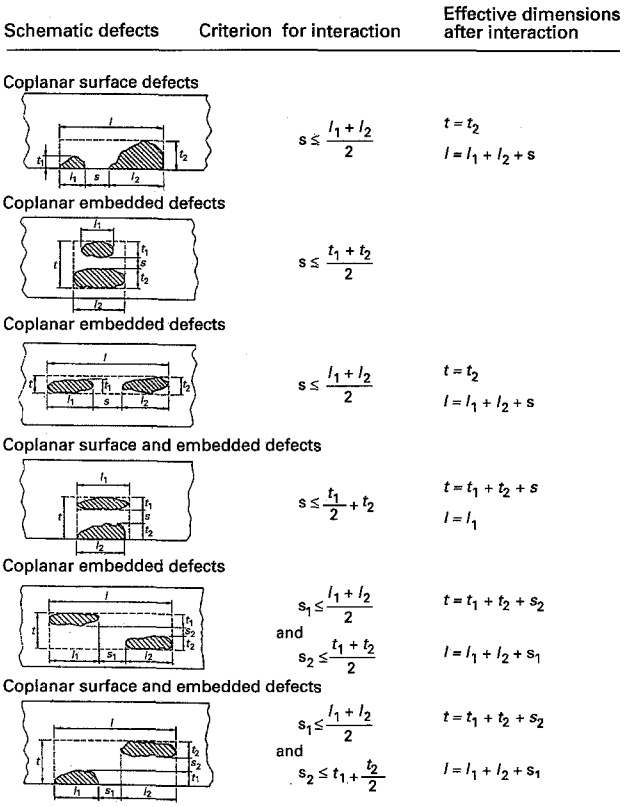


*Figure 6* Planar defect interaction rules [1].

composite equivalent defect results for the scale. The composite defects are normally expected to be of a certain size, which is a proportion of the oxide thickness, but infinitely long because interaction will occur in all

directions. Therefore, a shape parameter, $Q_0$ (which accounts for the ratio of void thickness to void length), and a membrane correction factor, $M_m$ (which accounts for the ratio of void size to overall size) have to be determined from the respective graphical representation of the functions of $Q_0$ and $M_m$. This allows $\hat{c}$ to be determined via

$$\pi\hat{c} = \frac{cM_m^2}{Q_0^2} \tag{30}$$

where $\hat{c}$ is an equivalent crack length, which represents the half-length of an idealized through thickness crack as shown in Fig. 7a which would have the same effect as the measured defect. Hence, a plot of the failure stress, $\sigma_c$, as a function of $1/(\pi\hat{c})^{1/2}$ should have $K_{IC}$ as slope and an intercept value which represents the residual stress. In this way Hancock and Nicholls [1] provided values of $K_{IC}$ for $FeO/Fe_3O_4$ on iron and $Cr_2O_3$ on Nimonic 75 ($\sim$ Ni–20%Cr). For both cases, $K_{IC}$ was insensitive to temperatures below 873 K, with a value of about 1.7 MN m$^{-3/2}$, but increased at higher temperatures.

However, the determination of $M_m$ required a very long extrapolation by a factor of 3 or more in the graphical representation. It was believed that this procedure involves too large an extrapolation for use with thin oxide layers because the procedure was developed for much larger structures, > 10 mm thick. Therefore, a slightly different approach was used, Nagl *et al.* [25, 26]. The interaction was considered critical only in the direction normal to the applied strains. Thus, the composite void size, $c$, could be obtained directly without extrapolation (Fig. 7b). However, the $K_{IC}$ values are expected to be smaller than those obtained with the extrapolation. In fact the observed $K_{IC}$-value for a $Fe_3O_4$/20% $Fe_2O_3$ scale on mild steel was $\sim$ 1.1 MN m$^{-3/2}$ at room temperature and at 823 K [25]. The values for nickel oxide were $\sim$ 0.41 and $\sim$ 1.61 MN m$^{-3/2}$ at room temperature and at 1173 K, respectively [26]. In both cases the tensile strain rate was $\sim 10^{-4}$ s$^{-1}$. Fig. 8 also shows the measured failure strains for iron oxide on mild steel as a function of oxide thickness and composite voids size [25]. The failure strains decreased with increasing oxide thickness. Similar observations were made by Hancock and Nicholls [1] and they thought that this was due to the higher probability of finding larger composite defects in thicker oxides. However, the data showed considerable scatter because the composite defects size was different in different samples of the same oxide thickness, i.e. the composite void size

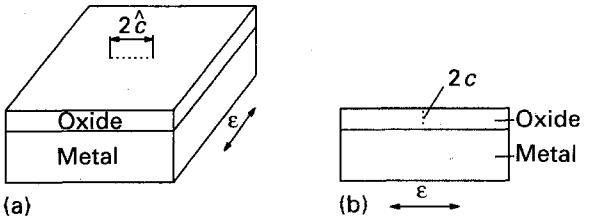


*Figure 7* Schematic diagram of (a) the idealised through-thickness crack in the surface oxide and (b) the crack size which was used by Nagl *et al.* [25, 26] without applying the extrapolation.

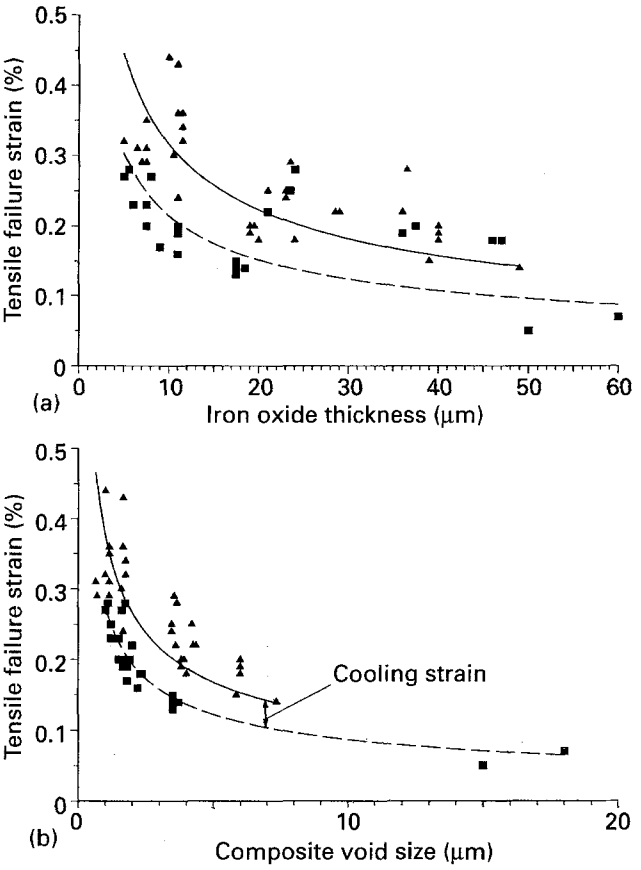


*Figure 8* Measured failure strains as a function of (a) thickness and (b) composite void size for iron oxides tested in tension at (—▲—) room temperature and at (– – ■ – –) 550 °C using a strain rate of $\sim 10^{-4}$ s$^{-1}$.

was not proportional to oxide thickness. Therefore, the failure strains were also plotted as a function of composite void size. This reduced the scatter considerably and the data followed closely the power law of the model predictions [25]. Thus, it seems apparent that the defect size is a crucial factor for the determination of the strength of oxide and this was also observed by Birchall *et al.* [52] for cement and by Rice [53] for bulk ceramics. It was also suggested that a major role of active element additions is to reduce the macro-defects present within the oxide scales with consequent benefit on scale adherence and spalling resistance [3, 10].

The last critical factors are the overall state of stress prior to the loading and the amount of lateral oxide growth, plasticity and creep of oxide and substrate during loading. Thus following relationship between the failure strain, $\varepsilon_c$ (which is calculated on the basis of a linear elastic fracture mechanics approach for a stress-free material) and the measured failure strain, $\varepsilon_m$, was used in [26]

$$\varepsilon_c = \varepsilon_m + \varepsilon_{gr} + \varepsilon_{cool} + \varepsilon_{pl} + \varepsilon_{lat} \tag{31}$$

where $\varepsilon_{gr}$ is the growth strain, $\varepsilon_{cool}$ is the cooling strain, $\varepsilon_{pl}$ is the strain compensated by time-dependent creep and $\varepsilon_{lat}$ is the strain compensated by lateral oxide growth which is only expected during deformation in tension [13]. $\varepsilon_{pl}$ and $\varepsilon_{lat}$ always act to increase the measured failure strain, hence they always have to be inserted with an opposite sign to $\varepsilon_m$. The amount of

lateral oxide growth or plasticity cannot be determined at present, but it is possible to define the minimum temperature and the maximum strain rate below which they might contribute to failure (see also Sections 3.1 and 3.2). However, there are methods available to determine $\varepsilon_{gr}$ and $\varepsilon_{cool}$. Good agreement between measured and calculated strains was found in by Nagl *et al.* [25, 26, 35] using Equation 31. Hence, the difference between the failure strains at room temperature and at 823 K (Fig. 8) was assumed to be a measure for the cooling stresses [25].

## 6. Conclusion

The preceding survey showed that there have been several attempts to model oxide failure. There has been general agreement for using fracture mechanics to model failure. The critical fracture mechanics parameters are the Young's modulus, the fracture surface energy of oxide and interface and the composite void size, which has been ignored until recently. However, the fracture mechanics models take only account of the linear elastic part of the deformation prior to the failure. Thus, it is necessary to include in any model factors which account for the effects of residual growth and cooling stresses prior to loading and factors which account for lateral oxide growth and creep of oxide and substrate during loading. In addition, the full potential of the models has not been explored because reliable data were not available for the critical parameters in the models, nor were measured failure strains available which could be used to verify the predictions. Certainly, the difficulties involved in measuring these parameters at growth temperature have contributed to the lack of data.

## Acknowledgements

The European Community provided financial support under the Brite/Euram-Program for Dr M. M. Nagl. The British Council provided a travel grant to visit research centres in Germany for M. M. Nagl and W. T. Evans. Special thanks to Dr S. R. J. Saunders and D. J. Hall, Division of High Temperature Meteorology, National Physical Laboratory, Teddington, UK, for the useful discussions and recommendations during writing this review.

## References

1. P. HANCOCK and J. R. NICHOLLS, *Mater. Sci. Technol.* **4** (1988) 398.
2. J. BARBEHÖN, "Das Verhalten von Oxidschichten auf Metallen bei Zug-, Druck- und zyklischer Verformung. Fortschritt-Berichte VDI Reihe 5 Nr 138" (VDI-Verlag, Germany, 1988).
3. J. R. NICHOLLS and S. R. J. SAUNDERS, in Surface Stability, edited by T. N. Rhys-Jones (Institute of Metals, London, 1990) pp. 95–144.
4. J. K. TIEN and J. M. DAVIDSON, in "Proceedings of the Symposium on Stress Effects and the Oxidation of Metals", edited by J. V. Cathcart (AIME, USA, 1974) pp. 200–219.
5. A. M. HUNTZ, *Mater. Sci. Technol.* **4** (1988) 1079.
6. J. STRINGER, *Corros. Sci.* **10** (1970) 513.
7. J. ARMITT, D. R. HOLMES, M. I. MANNING, D. B. MEADOWCROFT and E. METCALFE, Report FP-686 (Electric Power Research Institute (EPRI), Palo Alto, 1978).
8. M. I. MANNING, *Corros. Sci.* **21** (1981) 301.
9. *Idem*, in "Corrosion and Mechanical Stress at High Temperatures," edited by V. Guttmann and M. Merz (Applied Science, London, 1981) pp. 323–38.
10. J. ROBERTSON and M. I. MANNING, *Mater. Sci. Technol.* **6** (1990) 81.
11. M. WALTER, Doctoral thesis, Technische Hochschule Aachen, Germany (1991).
12. J. G. ZHAO and A. M. HUNTZ, *J. Mater. Sci.* **19** (1984) 3166.
13. M. SCHÜTZE, *Oxid. Metals* **24** (1985) 199.
14. *Idem, Int. J. Pres. Ves. Piping.* **47** (1991) 293.
15. *Idem, Mater. Sci. Technol.* **6** (1990) 32.
16. H. J. FROST and M. F. ASHBY, "Deformation-Mechanism Maps" (Pergamon Press, Oxford, 1982).
17. L. BERCHTOLD, H. G. SOCKEL and B. ILSCHNER, in "Behaviour of High Temperature Alloys in Aggressive Environments" (Metals Society, London, 1980) pp. 927–41.
18. M. SCHÜTZE, *Oxid. Metals* **25** (1986) 409.
19. M. SCHÜTZE and A. RAHMEL, in "Proceedings of the Conference on Corrosion in Coal Conversion Systems", edited by M. I. Manning and B. Meadowcroft (Applied Science, London, 1982) pp. 439–65.
20. H. COHRT and R. THÜMMLER, *Surf. Coat. Technol.* **32** (1987) 339.
21. S. R. J. SAUNDERS and J. R. NICHOLLS, *Mater. Sci. Technol.* **5** (1989) 780.
22. J. J. BARNES, J. G. GOEDJEN and D. A. SHORES, *Oxid. Metals* **32** (1989) 449.
23. H. E. EVANS, *Mater. Sci. Technol.* **4** (1988) 415.
24. M. M. NAGL, D. J. HALL and W. T. EVANS, in "Proceedings of the NACE Conference on Life Prediction of Corrodible Structures" (NACE, Houston, to be published).
25. M. M. NAGL, W. T. EVANS, D. J. HALL and S. R. J. SAUNDERS, *J. de Phys.* (1993) to be published.
26. M. M. NAGL, S. R. J. SAUNDERS, W. T. EVANS and D. J. HALL, *Corros. Sci.* **35** (1993) 965.
27. H. E. EVANS, *Mater. Sci. Eng.* **A120** (1989) 139.
28. S. OSGERBY and B. F. DYSON, *Mater. Sci. Technol.* **6** (1990) 2.
29. A. G. EVANS and R. M. CANNON, *Mater. Sci. Forum* **43** (1989) 243.
30. J. C. GROSSKREUTZ and M. B. McNEIL, *J. Appl. Phys.* **40** (1969) 355.
31. A. G. EVANS, G. B. CRUMLEY and R. E. DEMARAY, *Oxid. Metals* **20** (1983) 193.
32. H. RIEDEL, *Met. Sci.* **16** (1982) 569.
33. J. HEITZER, *Int. J. Fract.* **46** (1990) 271.
34. M. SCHÜTZE, *Mater. Sci. Eng.* **A121** (1989) 563.
35. M. M. NAGL, Doctoral thesis, University of Glamorgan, UK (1992).
36. C. H. WELLS, P. S. FOLLANSBEE and R. R. DILS, in "Proceedings of the Symposium on Stress Effects and the Oxidation of Metals", edited by J. V. Cathcart (AIME, USA, 1974) pp. 220–44.
37. H. E. EVANS and R. C. LOBB, *Corros. Sci.* **24** (1984) 209.
38. *Idem*, in "Proceedings of the 9th Congress on Metallic Corrosion" (NRC, Ottawa, 1984) pp. 46–53.
39. M. M. NAGL, W. T. EVANS, S. J. SAUNDERS and D. J. HALL, *Mater. Sci. Technol.* **8** (1992) 1043.
40. J. TIMOSHENKO and N. GOODIER, "Theory of Elasticity", 3rd Edn (McGraw-Hill, New York, 1969).
41. H. E. EVANS, G. P. MITCHELL, R. C. LOBB and D. R. J. OWEN, Report TD/FCB/REP/0070 (Nuclear Electric Plc., Berkeley, UK, 1990).
42. R. C. LOBB, J. A. SASSE and H. E. EVANS, *Mater. Sci. Technol.* **5** (1989) 828.
43. J. TADA, P. C. PARIS and G. R. IRWIN, "Stress Analysis of Cracks – Handbook" (Paris Productions, St Louis, 1974).
44. M. SCHÜTZE, in "Proceedings of the International Symposium on Solid State Chemistry of Advanced Materials", edited by Y. Saito, B Önay and T. Maruyama (Elsevier, Amsterdam, 1992).

45. H. E. EVANS and R. C. LOBB, in: "Proc. EUROCORR'87" (Dechema, Germany, 1987) pp. 135–40.
46. R. C. HURST, M. DAVIES and P. HANCOCK, *Oxid. Metals* **9** (1975) 161.
47. A. S. KHANNA, B. B. JHA and R. BALDEV, *ibid.* **23** (1985) 159.
48. W. CHRISTL, A. RAHMEL and M. SCHÜTZE, *Mater. Sci. Eng.* **87** (1987) 289.
49. *Idem, Oxid. Metals* **31** (1989) 35.
50. *Idem, ibid.* **31** (1989) 1.
51. A. G. EVANS and J. W. HUTCHINSON, *Acta Metall.* **37** (1989) 909.
52. J. D. BIRCHALL, A. J. HOWARD and K. KENDALL, *Nature* **289** (1981) 388.
53. R. W. RICE, *J. Mater. Sci.* **19** (1984) 895.
54. P. HANCOCK, in "Proceedings of the Symposium on Stress Effects and the Oxidation of Metals," edited by J. V. Cathcart (AIME, USA, 1974) pp. 155–76.
55. K. KATAOKA, T. YAMAZAWA, Y.-J. PYUN and T. HOMMA, *Trans. ISIJ* **24** (1984) 365.
56. J.C. PIVIN, J. MORVAN, D. MAIREY and J. MIGNOT, *Scripta Metall.* **17** (1983) 179.
57. C. LIU, A.-M HUNTZ and J.-L. LEBRUN, *J. de Phys.* (1993) to be published.

*Received 4 February 1992*
*and accepted 5 May 1993*